DOI https: //doi. org/10.1007/s11595-024-2883-9

Bio-inspired Hydroxyapatite/Gelatin Transparent Nanocomposites

TAN Junjun, WU Mingchen, LI Yuzhe, PENG Jiamei, XIONG Yan*

(Hubei Province Key Laboratory of Green Materials for Light Industry, Collaborative Innovation Center for Green Light-weight Materials and Processing, Hubei University of Technology, Wuhan 430068, China)

Abstract: Hydroxyapatite (HA) nanoparticles impart outstanding mechanical properties to organic-inorganic nanocomposites in bone. Inspired by the composite structure of HA nanoparticles and collagen in bone, a high performance HA/gelatin nanocomposite was first developed. The nanocomposites have much better mechanical properties (elongation at break 29.9%, tensile strength 90.7 MPa, Young's modulus 5.24 GPa) than pure gelatin films (elongation at break 9.3%, tensile strength 90.8 MPa, Young's modulus 2.5 GPa). In addition, the composite films keep a high transmittance in visible wavelength range from 0% to 60% of the HA solid content. These differences in properties are attributed to the homogeneous distribution of HA nanoparticles in the gelatin polymer matrix and the strong interaction between the particle surfaces and the gelatin molecules. This protocol should be promising for HA-based nanocomposites with enhanced mechanical properties for biomedical applications.

Key words: hydroxyapatite; nanocomposites; sodium citrate; gelatin; colloidal stability

1 Introduction

The mammalian bone is a unique case of natural nanocomposites, which are mainly HA nanoparticles highly homogeneously dispersed and with an oriented structure in the collagen matrix[1,2]. Because of this, the bone has outstanding mechanical properties that meet the mechanical performance needs of mammals throughout their lives[3]. Due to the great demand for human own health, especially for bone repair and bone replacement materials, and the expansion of polymer-based HA composites for bio-related applications, there is a great expectation to prepare nanocomposites with mechanical properties similar to those of bone[4-7].

In view of this, much effort has been put into the preparation of polymer-based HA nanocomposites[8]. HA/PLA nanocomposites was fabricated by an injection molding method, which SDS was used to improve the interfacial compatibility between HA and PLA. When the HA content of the nanocomposite is 10wt%, the nanocomposite is achieved the highest mechanical property [9]. HA/poly (methyl methacrylate) nanocomposites were prepared by free radical copolymerization of surface-modified HA with methyl methacrylate via a bulk copolymerization process. When 20wt% of HA was incorporated into the PMMA matrix, the glass transition temperature, thermal degradation temperature and tensile strength increased by 12 ℃, 52 ℃, and 76.2%, respectively, compared to the mother PMMA. However, higher HA content (20wt%) weakened the thermal and mechanical properties of the nanocomposites owing to the phase separation in the composite matrix caused by the strong aggregation of HA particles[10].

Although composites of HA nanoparticles with different polymers have been prepared, there are still some limitations[8,11]. For example, due to the small size of HA nanoparticles and the inherent polar solid surface, the particles exhibit a strong tendency to agglomerate[12]. In other words, when such particles are compounded into polymeric matrices, on the one hand the particles are mainly in the form of aggregates of different degrees rather than as individual particles. Even if the degree of agglomeration of the particles can be reduced by surface modification or surface grafting of the polymer, it is difficult to make all the

(Received: Mar. 26, 2023; Accepted: Sept. 18, 2023)

TAN Junun(谭军军): Assoc. Prof.; E-mail: tanjunjun2011@hbut.edu.cn

*Corresponding author: XIONG Yan(熊焰): Prof.; E-mail: xiongyan1980@hotmail.com

Funded by the Natural Science Foundation of Hubei Province (No. 2018CFB710), and the Opening Fund of Hubei Provincial Key Laboratory of Green Materials for Light Industry (No. 202107B07), Hubei University of Technology

particles uniformly dispersed as individual particles in the polymer matrix[13]. This will greatly reduce the effectiveness of the particle-polymer composite and reduce the overall contact area of the particles with the polymer.

Moreover, the particles are aggregated to a certain degree in the polymer matrix. In low particle concentration composites, the increase in particle addition is often beneficial to the strengthening of the mechanical properties of the composite. However, when the particle concentration is further increased, the increase of particle addition may not strengthen the mechanical properties, but may deteriorate the mechanical properties of the composite. In contrast, the weight solid content of skeletal HA is generally at least 60%, which is much higher than the effective solid content (3%-10%) of mechanical property enhancement of ordinary HA polymer nanocomposites. Therefore, the preparation of highly homogeneous HA polymer composites with high solid content remains a challenge so far.

In recent years, the preparation of HA nanoparticles based on sodium citrate-assisted hydrothermal method has been reported. By adjusting the sodium citrate to calcium molar ratio, the pH of the dispersion, the hydrothermal temperature and the hydrothermal time, HA nanoparticles with homogeneous size and shape can be prepared[14,15]. Due to the adsorption of citrate ions on the HA nanoparticles at the surface of the particles, the particles have a strong negative charge in aqueous media, presenting as individual nanoparticles dispersed in water. Meanwhile, using high-resolution solid-state NMR, it was found that natural bone contains a large amount of citrate molecules, with the vast majority distributed on the surface of HA nanoparticles[16]. Sodium citrate plays a crucial role in regulating the morphology, size and uniform distribution of HA nanoparticles in collagen[17-19].

Gelatin is a protein derived from collagen by controlled hydrolysis, which consists of a large number of glycine, proline, and 4-hydroxy proline residues. Gelatin has excellent biocompatibility, biodegradability[20]. Due to the abundance of hydroxyl, amino and carboxyl groups in the molecular structure of gelatin, it has both good water solubility and a large number of reactive groups that can interact with the solid surface of HA[21-24]. From this it is reasonable to assume that if the HA nanoparticles prepared by the sodium citrate-assisted hydrothermal method and the gelatin solution are mixed at a suitable pH, a more desirable homogeneous hybrid system can be obtained. When this system is applied to the preparation of nanocomposites, it is possible for the HA particles to remain dispersed as individual particles in the polymer matrix. At the same time the abundant carboxyl groups on the particle surface form hydrogen and ionic bonds with the hydroxyl, amino and carboxyl groups in the gelatin molecular structure, reinforcing the interfacial interactions between the HA solid particles and the polymer. The result is that the composite should have significantly enhanced mechanical properties and remain mechanically reinforced even when the particle solid content of the composite is close to the particle solid content of bone.

Although much previous work has been reported on polymer-based HA composites, homogeneous composites with high solids content have so far remained a challenge due to the agglomeration of nanoparticles and the lack of effective particle-polymer interactions[25,26]. In view of this, there is a great need for a simple, reproducible method of preparing high transparency composites.

Therefore, in this work, we firstly prepared HA nanoparticles that are homogeneous in size and shape and have good colloidal dispersion in water. Secondly, by solution mixing, the HA nanoparticles are co-blended with gelatin and dried after lay-up to form composites. Finally, the mechanical properties, transparency and structure of the material were characterized and analyzed.

2 Experimental

2.1 Materials

Calcium nitrate tetrahydrate ($Ca(NO_3)_2.4H_2O$, ⩾99.0%), sodium phosphate tribasic dodecahydrate ($Na_3PO_4.12H_2O$, ⩾98.0%), sodium citrate tribasic dihydrate ($C_6H_5Na_3O_7.2H_2O$, ⩾99.0%), gelatin (chemical purity), absolute ethanol (C_2H_6O, ⩾99.7%) and sodium hydroxide (NaOH, ⩾97.0%) were purchased from Shanghai Aladdin Reagent Co., Ltd. (Shanghai, China). All chemicals were used as received without further purification. Deionized water was used throughout the study.

2.2 Preparation of aqueous colloidal HA nanorod dispersions

In a typical experiment, an aqueous solution of sodium citrate (0.02 mole, 15 g H_2O) was slowly added to an aqueous solution of calcium nitrate (0.02 mole,

15 g H_2O) with continuous stirring over 10 min. Then, an aqueous solution of phosphate (0.012 mole, 30 g H_2O) was slowly added to the mixture with vigorous stirring over 10 min. After that, the as-obtained mixed solution was transferred to a Teflon-lined stainless-steel autoclave with a 100 mL capacity. The solution in the autoclave underwent hydrothermal treatment at 180 ℃ for 6 h. After hydrothermal treatment, the autoclave was cooled rapidly to room temperature with water, and the resulting product was purified using a three-cycle centrifugation-washing process with deionized water and ethanol.

Finally, the sample in dispersion form was obtained by redispersing the purified product in deionized water. The pH of the dispersion was adjusted to 9.5 by the addition of 0.1 M NaOH. The target mass fraction of the dispersion was achieved by controlling the mass of deionized water added. The sample in powder form was obtained by drying the purified product in the oven at 80 ℃ for 24 h.

2.3 Preparation of gelatin/HA nanocomposites

Gelatin/HA nanocomposites were fabricated via a casting method. Firstly, the HA colloidal dispersion with a mass fraction of 10wt% was mixed with gelatin powder under magnetic stirring to form a mixture with a target mass fraction. The mixture was then heated to 45 ℃ for 3 hours until the gelatin powder was completely dissolved. The mixture was then poured into the mold and flattened with a glass rod. The mold consists of two parts, the bottom part is PTFE plate, and the top part is stainless steel plate. The inner cavity area of stainless steel plate is 8 cm × 8 cm, and the thickness of the cavity is 1 mm. Finally, the mixture in the mold was dried at room temperature for 24 hours.

Table 1 Component ratios of the prepared samples

Sample code	HA/wt%	Gelatin/wt%
GHA0	0	100
GHA10	10	90
GHA20	20	80
GHA40	40	60
GHA60	60	40
GHA80	80	20

For the sake of simplicity, gelatin/HA nanocomposites fabricated under various experimental conditions will henceforth be labeled GHAx, where *x* is the weight ratio of HA to composite. For example, GHA10 refers to a composite with 10% HA solid content. The detailed experimental parameters are listed in Table 1.

2.4 Characterization

2.4.1 Wide-angle X-ray diffraction (XRD)

Powder X-ray diffraction was performed with an Empyrean Nano X-ray diffractometer (Panalytical, Holland) equipped with a Cu Kα radiation (0.15406 nm) source. Scans were performed from 10° to 80° with a scan rate of 6 °/min.

2.4.2 Transmission Electron Microscopy (TEM)

The morphology of the HA nanoparticles was inspected using a Transmission Electron Microscope (JEM-2100, JEOL) with an accelerating voltage of 200 kV. A sample of HA nanorod dispersion was pipetted and one or two drops were placed on the carbon side of a holey carbon-coated copper TEM-grid. The samples were then dried before being attached to the sample holder on the microscope.

In order to better describe the size characteristics of the synthesized HA nano nanoparticles, statistical analysis was used. The mean length <*L*> diameter <*D*> and aspect ratio< $R_{L/D}$ > of the HA nanoparticles were measured using a statistical method from three TEM images (at least 300 counts). The standard deviation of data is used to evaluate the dispersion of data. The calculation method was defined using the following equations:

$$< R_{L/D} >= \frac{\sum_{1}^{n} L/D}{n} \tag{1}$$

$$< L >= \frac{\sum_{1}^{n} L}{n} \tag{2}$$

$$\sigma_R = \frac{\sqrt{\frac{1}{n}\sum_{1}^{n}(R_{L/D} - < R_{L/D} >)^2}}{< R_{L/D} >} \tag{3}$$

$$\sigma_L = \frac{\sqrt{\frac{1}{n}\sum_{1}^{n}(L - < L >)^2}}{< L >} \tag{4}$$

$$\sigma_D = \frac{\sqrt{\frac{1}{n}\sum_{1}^{n}(D - < D >)^2}}{< D >} \tag{5}$$

where, <*L*>, <*D*>, and < $R_{L/D}$ > are the mean length, diameter and aspect ratio of the HA nanoparticles, respectively. The values σ_L, σ_D, and s_R are the standard

deviations of the length, diameter and aspect ratio of the HA nanoparticles, respectively.

2.4.3 Thermogravimetric analysis (TGA)

Thermogravimetric measurements were performed with a thermal gravimetric analyzer (Q500, TA Instruments, USA). The samples were heated in a flow of nitrogen (100 mL/min) using a platinum sample holder. The temperature range is from room temperature to 800 ℃, at a heating rate of 10 ℃/min.

2.4.4 Fourier-transform infrared spectroscopy (FTIR)

Fourier transform infrared spectroscopy was performed with a TENSOR II FTIR spectrophotometer (Bruker corporation, Germany) by the KBr method. Spectra were recorded between 400 and 4 000 cm^{-1}.

2.4.5 Zeta potential and dynamic light scattering measurements

Zeta potential and dynamic light scattering measurements were performed with a nano-ZS90 Zetasizer (Malvern instruments Ltd., Malvern, UK). The data were recorded and analyzed using Dispersion Technology Software v. 5.0 (Malvern Instruments). The pH of sample solutions was adjusted to 9.5 using 0.1 M NaOH solution, which was determined with a PB-10 pH meter (Sartorius AG, Goettingen, Germany) at 25°C. No additional electrolytes were added during the measurement.

2.4.6 Field-emission scanning electronic microscopy (SEM) analysis

The surfaces and crossed sections of composite films were observed by a scanning electron microscope (Hitachi SU-8010, Hitachi High Technologies, Japan). The SEM samples were coated with gold for 30 s, using a MSP-2S Magnetron sputter, before the SEM observations. Energy dispersion X-ray spectrometry (EDS) were performed at 10 kV with the Hitachi SU-8010 SEM and a X-Max instrument (Oxford Instruments), to analyze Ca and P elements in nanocomposites.

2.4.7 UV-Vis transmittance spectra

The light transmittance of specimens was measured with a spectrometer (U-3900, Hitachi, Japan) with a wavelength range of 200-800 nm. The specimens were cut to the size of about 2 cm×2 cm. Each specimen was tested at least three times at room temperature.

2.4.8 Differential scanning calorimetry (DSC)

The thermal properties of the nanocomposites were characterized with a DSC 8500 differential scanning calorimeter (PerkinElmer Inc., USA) under a flowing nitrogen atmosphere. The samples were firstly heated from 30 to 150 ℃ at a rate of 10 ℃ /min and maintained at this temperature for 2 min. The samples were then cooled to 30 ℃ at a rate of 10 ℃ /min, and again heated to 150 ℃ at the same heating rate to record the endothermic melting peak.

2.4.9 Mechanical properties

The tensile strength tests were performed with a testing machine (CMT4204, SANS, China). Dumbbell shaped specimens of width 4 mm and length 25 mm were prepared from the samples, and the tensile tests were conducted at a rate of 2 mm/min. The slope of the linear region of the stress-strain curve was used to determine the Young's modulus. To avoid the effects of moisture on the mechanical properties, the composite films were dried at 60 ℃ for 2 h before the tensile tests.

3 Results and discussion

3.1 Phase identification from XRD patterns

Inspired by bone and teeth, the formation of homogeneous composites of HA nanoparticles

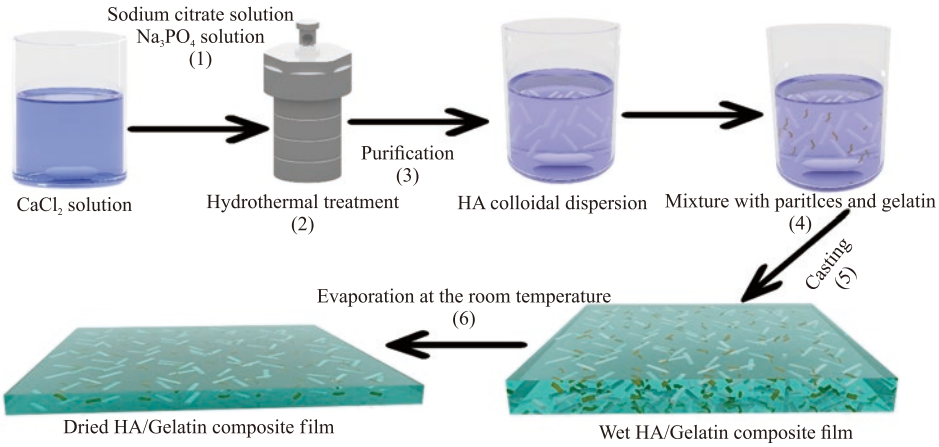

Fig.1 Schematic illustration of procedure for preparing HA-Gelatin nanocomposites

and natural macromolecules has been considered an important prerequisite for bone replacement materials, antimicrobial packaging materials and other extended applications. Our strategy involves five critical features, as shown in Fig.1: mixing of calcium, citrate and phosphate ions to form a mixture at room temperature, crystallization of the mixture by hydrothermal treatment, purification to obtain a stable HA colloidal dispersion, and mixing with gelatin to form homogenous mixture. casting the dispersion in the mold, and drying in the room temperature to form transparent composite film.

For the preparation of transparent gelatin/HA composites, the physical and chemical properties of the HA nanoparticles are crucial. The XRD pattern (Fig.2(a)) of the obtained particles displays the following diffraction peaks at 26.0°, 29.2°, 32.0°, 32.9°, 34.2°, 39.9°, 46.8°, 49.6°, 53.3°, and 64.1° which are correlated to the (h k l) indices (0 0 2), (2 1 0), (2 1 1), (1 1 2), (3 0 0), (3 1 0), (2 2 2), (2 1 3), (0 0 4), and (31 4) planes, respectively. All reflections are characteristics of the hexagonal phase of HA according to the standard data (JCPDS No. 74-0566) and reported in the Refs.[27, 28]. In addition, the profile of the diffraction peaks is integrated and sharp, indicating that the prepared particles are well crystallized.

The TEM image (Fig.2(b)) shows that the particles are rod-shaped, nanometer-sized and very homogeneous in shape. It is also noteworthy that the particles are loosely distributed in the TEM image, with no observable agglomerates, indicating good dispersion in aqueous media. The HRTEM image (Fig.2(c)) of HA nanoparticles show good crystallinity with the growth direction along c-axis and the lattice spacing of 0.34 nm, which is assigned to the (0 0 2) planes corresponding to the hexagonal HA.

In order to quantitatively characterize the dimension of the particles, the length, diameter and aspect ratio of over 200 particles from random three TEM images were statistically analyzed. The dimensional information (Figs.2(d)-2(f)) of the prepared HA nanoparticles was as follows: the average length was 75.26 nm with a standard deviation of 15.73 nm; the average diameter was 11.90 nm with a standard deviation of 2.81 nm; and the average aspect ratio was 6.39 with a standard deviation of 0.199.

Surface chemical composition of HA nanoparticles was determined by FTIR spectra (Fig.3(a)). The bands at 1 089, 1 033, 607, and 560 cm^{-1} can be attributed to the presence of P-O bonds of $PO4^{3-}$. The band at 3 573 cm^{-1} can be attributed to the presence of O-H bonds. The band at 1 382 cm^{-1} in the spectrum results from the presence of carboxyl groups.

The HA nanoparticles were also subjected to thermogravimetric measurements (Fig.3(b)). The weight loss (2.2%) of the samples below 200 ℃ is mainly attributed to the volatilization of trace water and water of crystallization. The weight loss (4.4%) of the samples between 200 and 800 ℃ is likely to have resulted from the thermal decomposition of

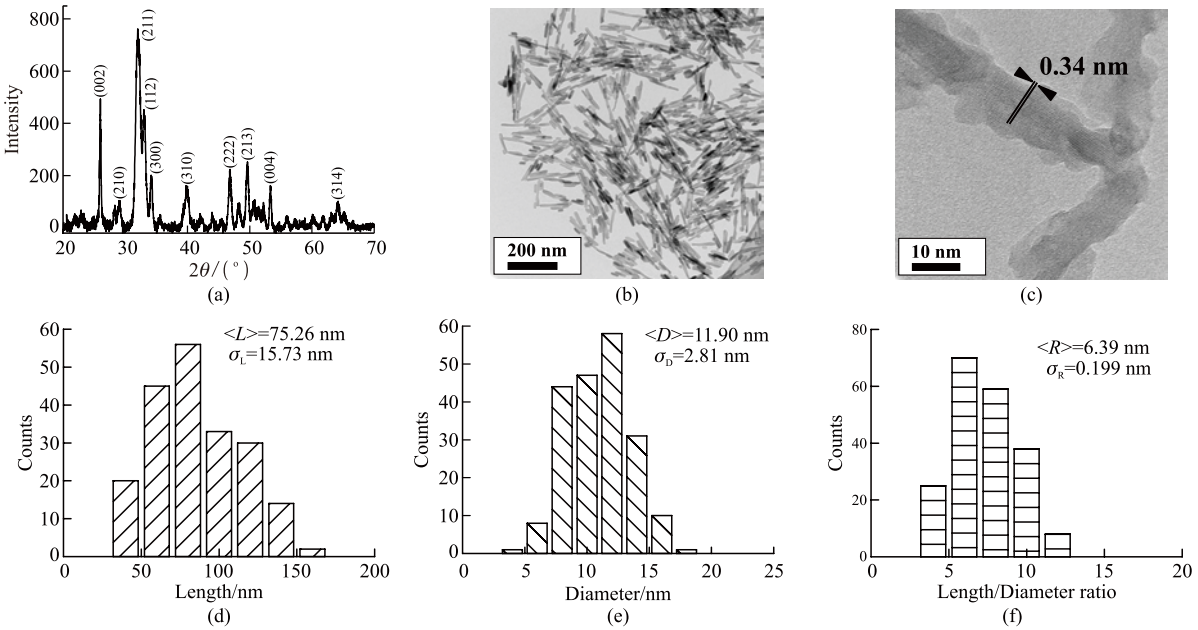

Fig.2 (a) XRD patterns, (b) TEM and (c) HRTEM images of particles; (d) Specific statistical information on the length; (e) Diameter; (f) Aspect ratio of the particles

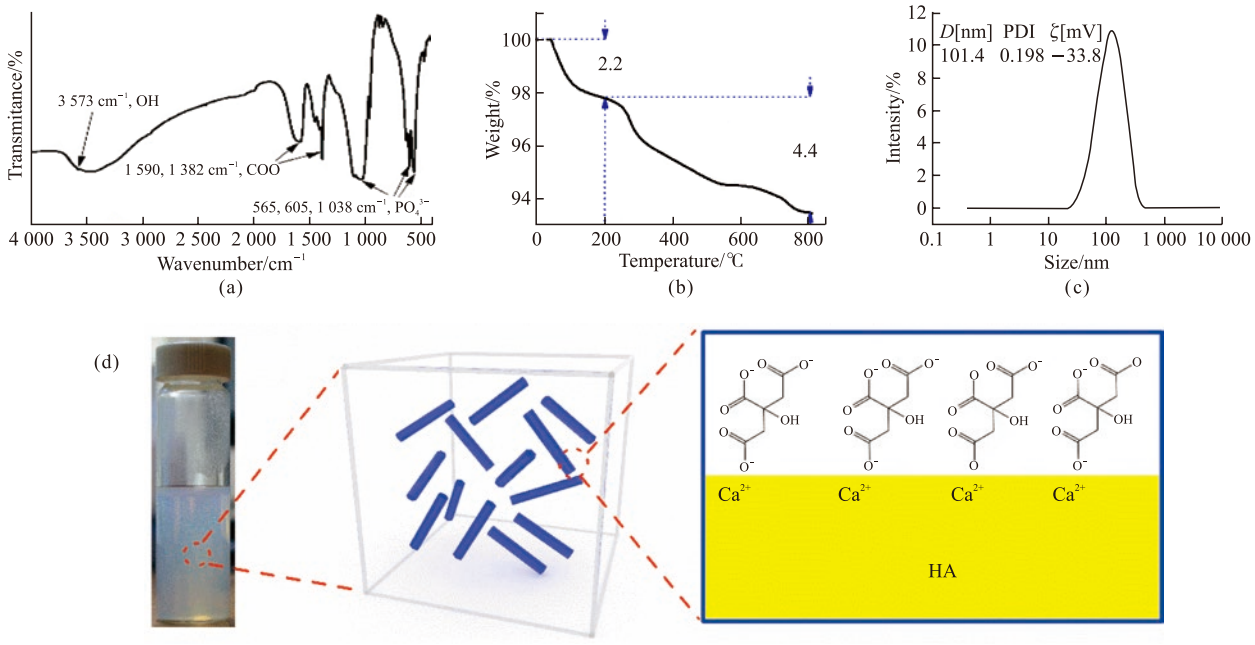

Fig.3 (a) FTIR spectra, (b) TG curve, (c) DLS of the HA nanoparticles and (d) a proposed diagram of the HA nanoparticles with an abundance of citrate molecules

citrate molecules adsorbed on the particle surface. The weight loss of the HA nanoparticles from 200 to 800 ℃ confirmed a strong absorption peak in the FTIR results at 1 600 cm^{-1}, indicating that an abundance of citrate molecules is adsorbed on the surface of HA nanoparticles.

As the prepared HA nanoparticles are nano-sized, homogeneous in shape and adsorb dense citrate molecules on the surface of the particles, it is assumed that the particles should be colloidally stable in aqueous solutions. To evaluate the colloidal stability of HA nanoparticles in aqueous phase, the DLS and zeta potential value measurements were conducted (Fig.3(c)). The zeta potential value is −33.8 mV and *Z*-average size is 101.4 nm, when pH of dispersion is 9.5 and particle concentration is 1wt%, suggesting that the HA nanoparticles are colloidally stable in aqueous medium.

Based on the aforementioned results, and in particular the comparison of the <*L*> and *Z*-average hydrodynamic diameter of the HA nanoparticles, a proposed diagram was established (Fig.3(d)). With the aid of the sodium citrate-assisted hydrothermal method, the particles are imparted a rod-like shape and uniform nano-size, while a large quantity of sodium citrate molecules are adsorbed on the surface of the particles. Due to the strong electrostatic repulsion, the nanoparticles are probably distributed in the aqueous medium as a single particle in aqueous phase. Because of this, the dispersion formed by the particles is transparent.

3.2 the properties of HA/Gelatin nanocomposites

Next, the HA dispersion was mixed with the gelatin to form a composite film. Nanocomposites with different HA solid content were prepared by regulating the weight ratio of the HA particles to the composite, with solid content ranging from 0% to 80%. Firstly, the effect of HA solid content on the transparency of the composite film was evaluated by UV-visible spectroscopy (Fig.4(a)).

The pure gelatin film is transparent with a high transmittance at visible-light region (>55% at wavelength 600 nm). Varying the solid content in the range of 0-60% does not significantly reduce the transparency of the composite films compared to the pure gelatin film. It is of interest that at 10% and 60% solid content, the transparency of the prepared composite films even exceeds that of the pure gelatin films. However, when the solid content reaches 80%, the transmittance of the composite film decreases significantly (<40% at wavelength 600 nm). Changes in the transparency of the composite films can also be directly observed by eye, as shown in Fig.4b. As can be seen from the images of the composite film, when the solid content of the composite film is between 0% and 60%, the composite film looks transparent. However, when the solid content reaches 80%, the composite film looks slightly white and less transparent.

The high transparency of the composite may

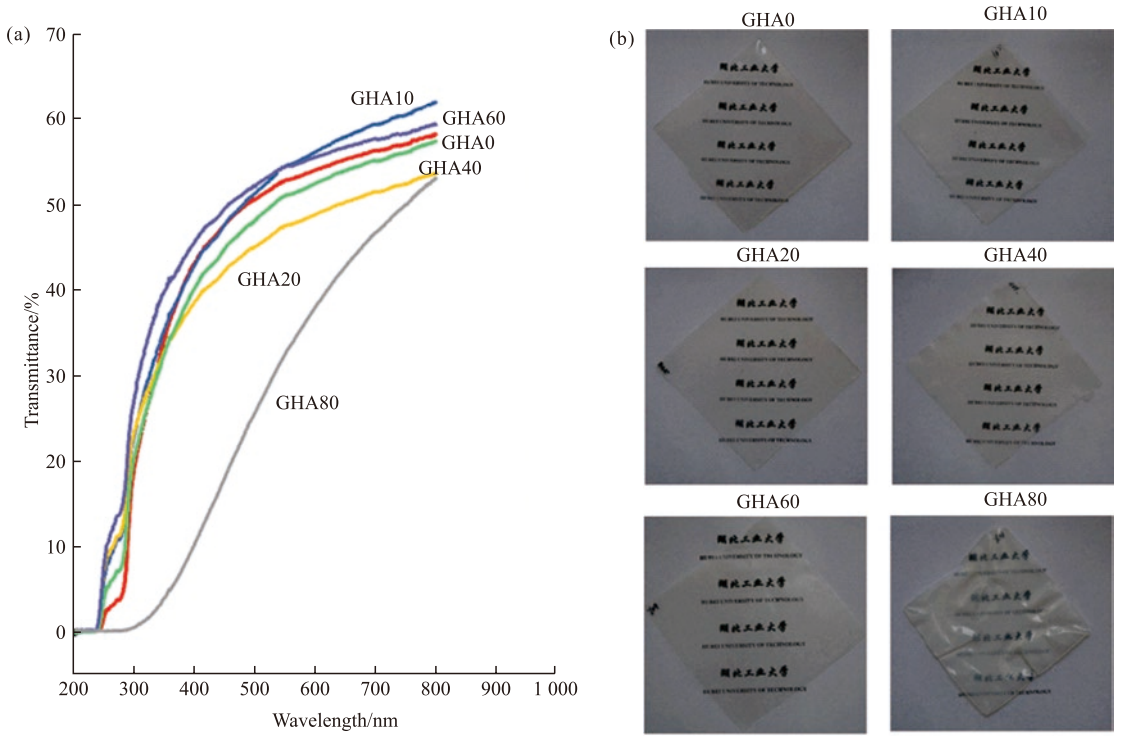

Fig.4 UV-Vis spectra (a) and photographs (b) of HA/Gelatin composites at different HA solid contents. All film samples are square with 8 cm sides

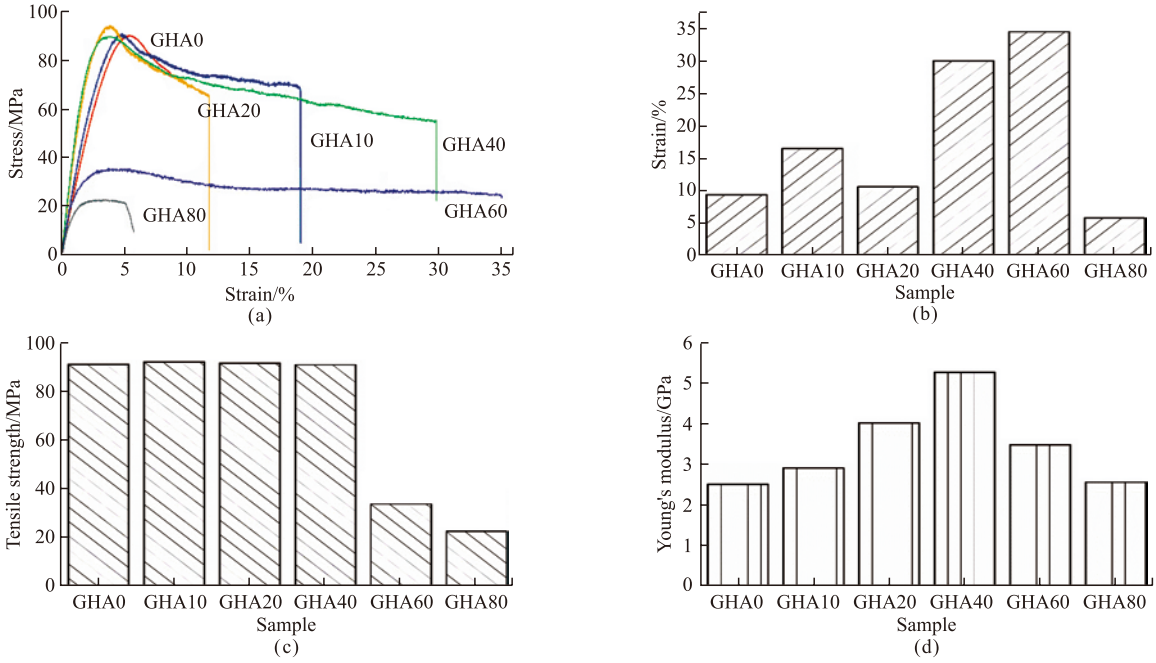

Fig.5 Mechanical properties of HA/gelatin composites: (a) Tensile stress-strain curves; (b) Tensile fractured strain tendency chart; (c) Tensile strength tendency chart; (d) Tensile Young's modulus tendency chart

reasonably be explained as follows: the intrinsic refractive index of HA with a value of 1.64-1.65[29] is very close to that of gelatin with a value of 1.5[30], reducing the scattering of light by the composite. The HA nanoparticles are probably distributed in the composite as individual particles in the polymer matrix, and the intrinsic size of the particles is smaller than the half-wavelength of light, causing no significant obstruction to the propagation of visible light. The HA nanoparticles do not have any form of aggregation, so there is no significant reflection of light.

The effect of HA solid content on the mechanical properties of the composite film was assessed by tensile testing. Figs.5(a)-5(d) show the stress-strain curve and

the variation in elongation at break, tensile strength and Young's modulus for the composites with HA solid content. A summary of the mechanical properties of the nanocomposites is also given in Table 2.

Table 2 Mechanical properties of the HA/gelatin composites at different HA solid contents

Sample	Tensile property					
	Strength /MPa	Increase /%	Modulus /GPa	Increase /%	Elongation /%	Increase /%
GHA0	90.8	-	2.50	-	9.3	-
GHA10	91.9	1.21	2.88	15.2	16.4	76.34
GHA20	91.3	0.55	3.99	59.6	10.5	12.90
GHA40	90.7	−0.11	5.24	109.6	29.9	221.50
GHA60	33.46	−63.15	3.45	38.0	34.36	269.46
GHA80	22.2	−75.55	2.55	2.0	5.7	−38.71

The elongation at break, tensile strength and Young's modulus of the pure gelatin film was 9.3%, 90.8 MPa, and 2.5 GPa, respectively. The tensile strength of the composite film, when the solid content increases from 0% to 40%, remains almost constant at around 90 MPa, with only 1-2 MPa fluctuations. As the solid content increases further, the tensile strength of the composite film decreases rapidly, with a tensile strength of only 22.2 MPa at a solid content of 80%.

The elongation at break of the composite films increase from 9.3% to 34.36% as the solid content increases from 0% to 60%. Further increasing the solid content to 80%, the elongation at break of the composite film drops sharply to 5.7%. As the solid content was increased from 0% to 80%, the Young's modulus of the composite films shows a similar trend to the elongation at break, but the maximum peak occurred in the sample with 40% solid content at a value of 5.24 GPa.

Compared to the mechanical properties of the pure Gelatin film as shown in Table 2, the tensile strength of the composite films shows little loss even when the solid content is increased to 40%; elongation at break increases by almost 221.50% at 40% solid content; and Young's modulus increases by 109.6% at 40% solid content.

3.3 Analysis of HA/gelatin nanocomposites

So far, based on data on the mechanical properties and transparency of the composites, it is recognized that the addition of HA nanoparticles significantly enhances the mechanical properties of the HA/Gelatin composites and maintains the high transparency of the HA/Gelatin composites even at higher solid contents.

In the following section, the HA/Gelatin composites were characterized to clarify how they are reinforced and how transparency is maintained. Fig.6 shows the crystalline structure and phase composition of HA/Gelatin composites. The pure gelatin film (GHA0) was amorphous phase without any observable diffraction peaks. As the amount of HA nanoparticles incorporated into the gelatin matrix increases, the HA diffraction peaks appear in the diffraction pattern of the composite film and the intensity of the diffraction peaks is gradually increased, which indicates that HA nanoparticles successfully incorporated into the gelatin matrix and HA nanoparticles homogenously distributed in the Gelatin matrix.

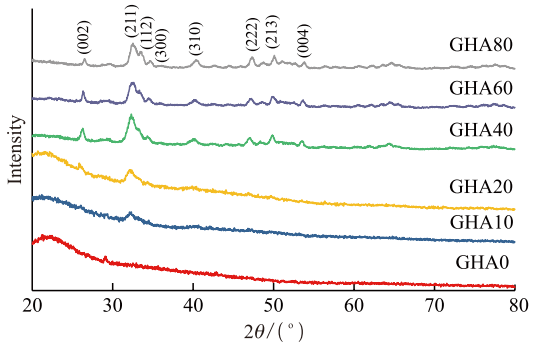

Fig.6 XRD patterns of HA/Gelatin composites at different HA solid contents

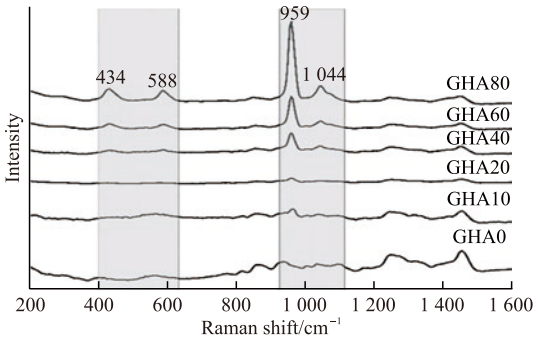

Fig.7 Roman spectra of HA/Gelatin composites at different HA solid contents

Fig.7 shows Raman spectra of HA/Gelatin composites with different solid contents. For the pure gelatin film, no characteristic peaks associated with HA can be observed in the Raman spectrum. As the HA solid content of the composites gradually increases, the characteristic peaks of HA appear and intensify, which are the phosphate modes at 1044 cm^{-1} ($\nu_3(PO_4^{3-})$), 959 cm^{-1} ($\nu_1(PO_4^{3-})$), 588 cm^{-1} ($\nu_4(PO_4^{3-})$), and 434 cm^{-1} ($\nu_2(PO_4^{3-})$). The appearance of these peaks and the trend in intensity with particle addition indicate the presence and uniform distribution of HA in the composite which is in accordance with XRD results.

DSC analysis was performed to analyze the effect of HA nanoparticle incorporation on the thermal properties of the composites, as shown in Fig.8. The pure gelatin film shows an endothermic peak centered at 97.8 ℃, associated with the helical-coil transition of gelatin[24]. As the HA nanoparticles are incorporated into the gelatin polymer matrix, the glass transition temperature of the composites shows a trend of first decreasing (93.4 ℃ for GHA10) and then gradually increasing (98.7 ℃ for GHA20, 98.3 ℃ for GHA40, 97.6 ℃ for GHA60, and 105.6 ℃ for GHA80). This implies that the addition of HA nanoparticles may reduce the thermal stability of the composite film at low solid content, which is mainly attributed to the disruption of the distribution of the original hydrogen bonds caused by the introduction of HA nanoparticles. When the solid content is further increased, the thermal stability of the composite films is enhanced, which is mainly attributed to the difficulty of molecular conformational transition caused by the large number of HA nanoparticles.

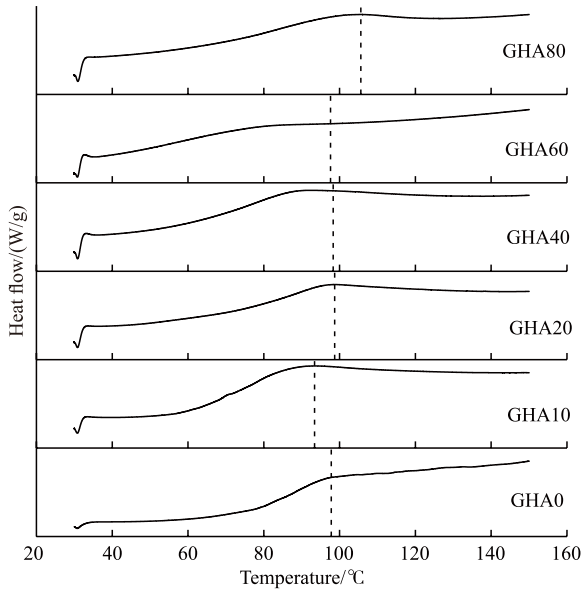

Fig.8 DSC curves of HA/Gelatin composites at different HA solid contents. The DSC results were obtained from second heating scan at a heating rate of 10℃ /min

The composite structures of the composites were examined by SEM observation of the surface and cross-section of HA/Gelatin composites at various solid content as shown in Figs.9(a)-9(f). The surface of the composite films remained flat and smooth before and after the addition of the HA particles, with no observable particle aggregation, indicating that the particles were uniformly distributed in the horizontal direction of the films. In terms of the cross-section of the composite films (Figs.9(a1)-9(f1)), before and after the addition of the HA particles, the fracture surface of the composite films remains flat and smooth, with no observable particle aggregates or holes, indicating that the film is dense and the particles are uniformly distributed in the fracture direction.

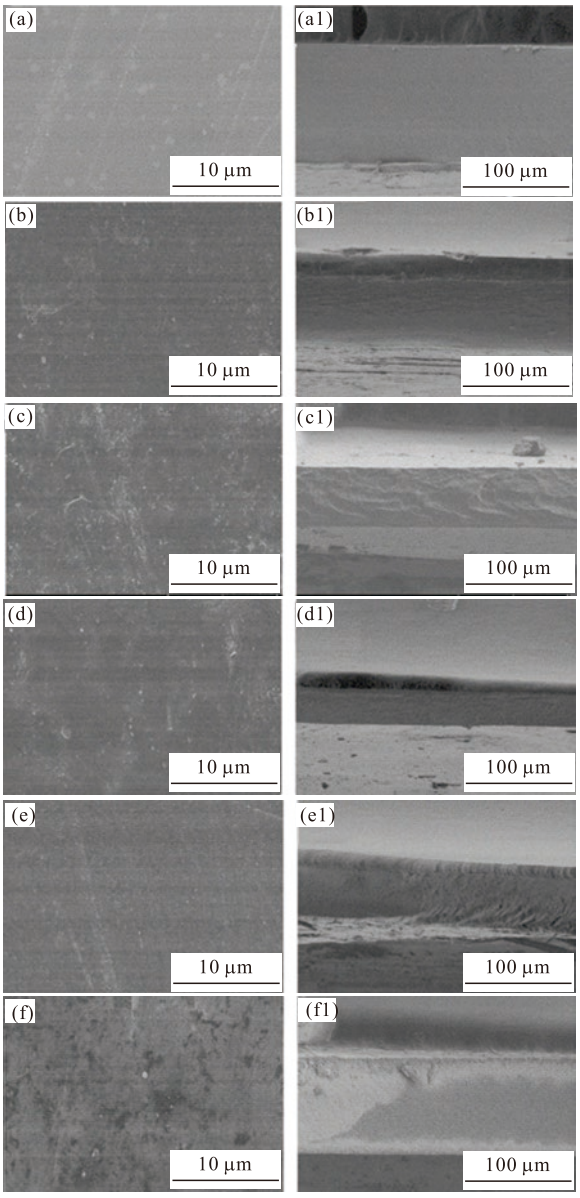

Fig.9 SEM images of HA/Gelatin composites at different HA solid contents. The letters a-f and a1-f1 represent the surface and cross-section of composites at solid content of 0, 10wt%, 20wt%, 40wt%, 60wt%, and 80wt%, respectively

To further illustrate the uniformity of particle distribution across the cross-section of the composite film, elemental analysis was carried out using energy dispersive X-ray spectroscopy (EDS), as shown in Fig.10. For a pure gelatin film, the presence of calcium and phosphorus is not detected in the elemental

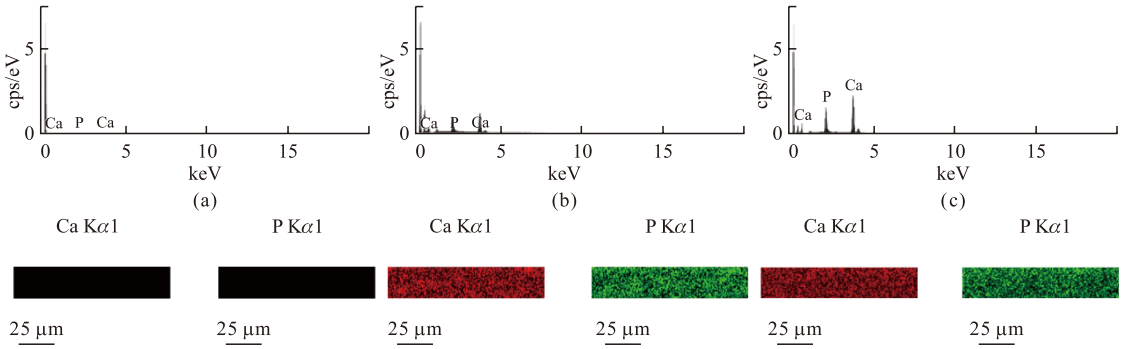

Fig.10 Ca and P Kα X-ray elemental mapping of the cross section of composites: (a) GHA0, (b) GHA20, and (c) GHA40

analysis, mainly because gelatin itself does not contain the elements calcium and phosphorus. As the HA solid content of the composites increases, excitation peaks for calcium and phosphorus elements appear and intensify, indicating that HA nanoparticles are successfully introduced into the gelatin polymer matrix. The patterns of calcium and phosphorus mapping show that the intensity of elements is not only enhanced with the increase of HA solid content, but also the elements are very uniformly distributed over the range examined, indicating that there is no agglomeration of the HA particles in any form in the cross-sectional direction of the composite films and no gradient settling, which is very similar to the reported work of amorphous calcium carbonate transparent composites[31].

The results of the mechanical properties of the composite films show that the prepared HA nanoparticles incorporated into the gelatin matrix are very effective in improving the mechanical properties of the composites. The mechanical strength of the composites after the addition of HA nanoparticles is on the one hand mainly attributed to the carboxyl groups on the surface of the particles. The gelatin molecule itself is a typical protein, rich in amino and carboxyl groups, and the carboxyl groups on the surface of the particles can be bound to the amino groups on the gelatin molecule chain in a coordination or electrostatic interaction. The carboxyl groups on the surface of the particles can also form hydrogen bonds with the hydroxyl groups on the gelatin chains. It is due to these interactions that the interfacial bonding between the HA nanoparticles and the gelatin matrix is enhanced. On the other hand, the particles have a strong electrostatic repulsion between them due to the abundance of carboxyl groups on their surface, giving them a homogeneous dispersion in the gelatin matrix.

However, excessively high particle additions (*eg*, 80% solid content) can significantly reduce the mechanical properties of the composite and make it fragile. This may be due to the fact that at low particle concentrations the particles are present as a dispersed phase and the polymer molecules as a continuous phase; after a high particle concentration (*eg*, 80% solid content) this distribution of particles with gelatin molecules may break down and there may be a portion of particles with no gelatin molecules between them. As the direct particle-particle interaction is much less than in the previous model, this leads to a fragile composite. These results suggest that no domain boundaries are formed at macroscale in the composite films. Because of this homogeneous structure, the composite films exhibit no light scattering and high transparency.

4 Conclusions

Inspired by the composite structures in bone, transparent composite films which are composed of the HA nanoparticles and gelatin, were fabricated by the solution method. As the solid content of the particles increases, the mechanical properties of the composite film are significantly enhanced and the transparency remains high. This change in properties can be attributed to two main factors: firstly, the sodium citrate imparts a strong negative charge to the HA nanoparticles, resulting in strong interparticle repulsion to prevent agglomeration and homogeneous distribution in the gelatin polymer matrix; secondly, the abundance of citrate molecules adsorbed on the surface of the particles provides a basis for the formation of more interaction (*eg*, hydrogen bonding) sites with gelatin molecules. This approach can be easily applied to the preparation of various water-soluble polymer-based HA nanocomposites to meet the requirements for mechanical properties and particle solid content for biologically relevant applications of these composites.

Conflict of interest

All authors declare that there are no competing interests.

References

[1] Weiner S, Wagner HD. The Material Bone: Structure-Mechanical Function Relations[J]. *Annual Review of Materials Science*, 1998, 28(1): 271-298

[2] Qi C, Musetti S, Fu LH, Zhu Y, Huang L. Biomolecule-assisted Green Synthesis of Nanostructured Calcium Phosphates and Their Biomedical Applications[J]. *Chem. Soc. Rev*., 2019, 48(10): 2 698-2 737

[3] Launey ME, Buehler MJ, Ritchie RO, On the Mechanistic Origins of Toughness in Bone[J]. *Annual Review of Materials Research*, 2010, 40(1): 25-53

[4] Habraken W, Habibovic P, Epple M, *et al*. Calcium Phosphates in Biomedical Applications: Materials for the Future[J]. *Materials Today*, 2016, 19(2): 69-87

[5] Guan QF, Ling ZC, Han ZM, *et al.* Ultra-Strong. Ultra-Tough, Transparent, and Sustainable Nanocomposite Films for Plastic Substitute[J]. *Matter.*, 2020, 3(4): 1 308-1 317

[6] Zhao C, Zhang P, Zhou J, *et al.* Layered Nanocomposites by Shear-flow-induced Alignment of Nanosheets[J]. *Nature*, 2020, 580(7802): 210-215

[7] Zhao H, Liu S, Wei Y, *et al.* Multiscale Engineered Artificial Tooth Enamel[J]. *Science*, 2022, 375(6580): 551-556

[8] Venkatesan J, Kim SK. Nano-hydroxyapatite Composite Biomaterials for Bone Tissue Engineering-A Review[J]. *J. Biomed. Nanotechnol*., 2014, 10(10): 3 124-3 140

[9] Huang Z, Wan Y, Peng M, *et al.* Incorporating Nanoplate-like Hydroxyapatite into Polylactide for Biomimetic Nanocomposites via Direct Melt Intercalation[J]. *Composites Science and Technology*, 2020, 185: 107 903

[10] Yang B, Li M, Wu Y, *et al.* Preparation and Characterization of Bone-like Hydroxyapatite/poly(methyl methacrylate) Composite Biomaterials[J]. *Science and Engineering of Composite Materials*, 2012, 0(0): 1-7

[11] Šupová M, Martynková GS, Barabaszová K. Effect of Nanofillers Dispersion in Polymer Matrices: A Review[J]. *Science of Advanced Materials*, 2011, 3(1): 1-25

[12] Supova M. Problem of Hydroxyapatite Dispersion in Polymer Matrices: A Review[J]. *J. Mater. Sci. Mater. Med*., 2009, 20(6): 1201-1 213

[13] Haojie D, Liuyun J, Bingli M, *et al.* Preparation of a Highly Dispersed Nanohydroxyapatite by a New Surface-Modification Strategy Used as a Reinforcing Filler for Poly(lactic-co-glycolide)[J]. *Industrial & Engineering Chemistry Research*, 2018: 57(50): 17 119-17 128

[14] Jin X, Chen X, Cheng Y, *et al.* Effects of Hydrothermal Temperature and Time on Hydrothermal Synthesis of Colloidal Hydroxyapatite Nanorods in the Presence of Sodium Citrate[J]. *J. Colloid Interface Sci.*, 2015, 450: 151-158

[15] Jin X, Zhuang J, Zhang Z, *et al.* Hydrothermal Synthesis of Hydroxyapatite Nanorods in the Presence of Sodium Citrate and Its Aqueous Colloidal Stability Evaluation in Neutral pH[J]. *J. Colloid. Interface Sci*., 2015, 443: 125-30

[16] Hu YY, Rawal A, Schmidt-Rohr K. Strongly Bound Citrate Stabilizes the Apatite Nanocrystals in Bone[J]. *Proc. Natl. Acad. Sci. USA*, 2010, 107(52): 22 425-22 429

[17] Delgado-Lopez JM, Bertolotti F, Lyngso J, *et al.* The Synergic Role of Collagen and Citrate in Stabilizing Amorphous Calcium Phosphate Precursors with Platy Morphology[J]. *Acta Biomater*., 2017, 49: 555-562

[18] Wang Z, Xu Z, Zhao W, *et al.* Isoexergonic Conformations of Surface-Bound Citrate Regulated Bioinspired Apatite Nanocrystal Growth[J]. *ACS Appl Mater Interfaces*, 2016, 8(41): 28 116-28 123

[19] Santos C, Almeida MM, Costa ME. Morphological Evolution of Hydroxyapatite Particles in the Presence of Different Citrate:Calcium Ratios[J]. *Crystal Growth & Design*, 2015, 15(9): 4 417-4 426

[20] Veis A. The Physical Chemistry of Gelatin[J]. *Int. Rev. Connect. Tissue Res.*, 1965, 3: 113-200.

[21] Bigi A, Panzavolta S, Roveri N. Hydroxyapatite-gelatin Films: A Structural and Mechanical Characterization[J]. *Biomaterials*, 1998, 19(7-9): 739-744

[22] Chang MC, Ko CC, Douglas WH. Preparation of Hydroxyapatite-gelatin Nanocomposite[J]. *Biomaterials*, 2003, 24(17): 2 853-2 862

[23] Teng S, Shi J, Peng B, *et al*. The Effect of Alginate Addition on the Structure and Morphology of Hydroxyapatite/Gelatin Nanocomposites[J]. *Composites Science and Technology*, 2006, 66(11-12): 1 532-1 538

[24] Wu X, Liu Y, Wang W, *et al*. Improved Mechanical and Thermal Properties of Gelatin Films Using a Nano Inorganic Filler[J]. *Journal of Food Process Engineering*, 2017, 40(3): 1-10

[25] Zhang R, Hu H, Liu Y, *et al.* Homogeneously Dispersed Composites of Hydroxyapatite Nanorods and Poly(lactic acid) and Their Mechanical Properties and Crystallization Behavior[J]. *Composites Part A: Applied Science and Manufacturing*, 2020, 132: 105 841

[26] Tan J, Jin X, Chen M. Bio-inspired Synthesis of Aqueous Nanoapatite Liquid Crystals[J]. *Sci. Rep*., 2019, 9(1): 466

[27] Tan J, Liu Y, Gong J, *et al*. Non-aqueous Liquid Crystals of Hydroxyapatite Nanorods[J]. *Acta Biomater*., 2020, 116: 383-390

[28] Chen X, Jin X, Tan J, *et al.* Large-scale Synthesis of Water-soluble Luminescent Hydroxyapatite Nanorods for Security Printing[J]. *J. Colloid. Interface Sci.*, 2016, 468: 300-306

[29] Dou L, Zhang Y, Sun H. Advances in Synthesis and Functional Modification of Nanohydroxyapatite[J]. *Journal of Nanomaterials*, 2018, 2018: 1-7

[30] Tan KM, Tjin SC, Chan C, *et al.* High Relative Humidity Sensing Using Gelatin-coated Long Period Grating[J]. *Proceedings of SPIE*, 2005, 5 855: 375-378

[31] Kuo D, Nishimura T, Kajiyama S, *et al.* Bioinspired Environmentally Friendly Amorphous $CaCO_3$-Based Transparent Composites Comprising Cellulose Nanofibers[J]. *ACS Omega*., 2018, 3(10): 12 722-12 729